Journal of Thermal Analysis and Calorimetry (2020) 141:1619–1633
https://doi.org/10.1007/s10973-020-09661-4

Investigation of porous media effects on lithium-ion battery thermal management

Amirreza Kaabinejadian[1] · Hesam Ami Ahmadi[1] · Mahdi Moghimi[1]

Received: 7 February 2020 / Accepted: 1 April 2020 / Published online: 20 April 2020

Abstract

The utilization of porous media and its effects on thermal management of internally cooled lithium-ion battery with the aid of porous media has been investigated. Two different configurations of the porous zone have been studied through three-dimensional transient thermal analysis of prismatic lithium-ion battery with liquid electrolyte as a coolant. At first, both configurations of the porous zone were investigated in pursuit of detecting the optimum configuration. Afterward, the effects of various materials, porosities and pores sizes were explored on the standard deviation of the temperature field and maximum temperature inside the battery in the optimum porous zone configuration. In the end, the utilization of the response surface method due to the parametric study and discover the most crucial parameters in battery performance was scrutinized. Compared to the non-inclined porous, the inclined porous zone case decreases the standard deviation of the temperature field significantly. Using the inclined porous zone also indicates that decreasing porosity results in the enhancement of both maximum temperature and standard deviation of the temperature about 20.75%. Hence, the increment of pore size results in decreasing maximum temperature inside the battery, while it could help the standard deviation of the temperature to be improved by about 24.88%.

Keywords Lithium-ion battery pack · Porous media · Internal cooling · Thermal management · Hybrid electric vehicle

List of symbols

p_∞	Ambient pressure (kPa)
C_0	Battery capacity
h_c	Convection coefficient (W m^{-2} K^{-1})
V	Voltage of cell (V)
Da	Darcy number
I	Discharge current (A)
i	Discharge current per unit volume (A m^{-3})
ΔS	Entropy generation (J mol^{-1} K^{-1})
E	Energy (kJ)
F	Faraday number (C mol^{-1})
D_h	Hydraulic diameter
$\dot{Q}$	Heat generation rate (W)
p_{in}	Inlet pressure (kPa)
u_{in}	Inlet velocity (m s^{-1})
A_{in}	Inlet area (m^2)
R_i	Internal equivalent resistance of unit volume (Ω m^3)
C	Inertial resistance (m^{-1})
ν	Kinematic viscosity (m^2 s^{-1})
Nu	Nusselt number
p_{out}	Outlet pressure (kPa)
U	Open-circuit voltage (V)
Pr	Prandtl number
P	Pumping power (W)
K	Permeability
Re	Reynolds number
p_{static}	Static pressure (kPa)
S_f^h	Source term
α	Thermal diffusivity (m^2 s^{-1})
T	Temperature (K)
k	Thermal conductivity (W m^{-1} K^{-1})
t	Time (s)
$\dot{V}$	Volumetric flow rate (m^3 s^{-1})
v	Velocity (m s^{-1})
D	Viscous resistance (m^{-2})

Greek letters

ρ	Density
γ	Porosity
$\overline{\overline{\tau}}$	Stress tensor
λ	Thermal conductivity

✉ Mahdi Moghimi
moghimi@iust.ac.ir

[1] School of Mechanical Engineering, Iran University of Science and Technology, Narmak, Tehran, Iran

$\vec{v}$ Velocity tensor
μ Viscosity

Subscripts

P Porous
np Non-porous
in Inlet
S Solid
f Fluid

Abbreviations

CS Carbon steel
CE Cooling efficiency
LIB Lithium-ion battery
PP Pumping power
PCM Phase change material
PS Pore size
PO Porosity
SOC State of charge
STD Standard temperature deviation

Introduction

Nowadays, using batteries can be very useful to supply the required energy due to their energy density and zero-emission. Fossil fuels have hazardous influence and could jeopardize human life. Lithium-ion battery, LIB, is one kind of rechargeable batteries, which have various applications in hybrid electric vehicles, mobile, laptop and other electronic devices. LIBs have a high energy density that can produce high energy in a low volume. Lithium-ion batteries are susceptible to the temperature inside the battery. These kinds of batteries are available on three different shapes such as pouch, cylindrical and prismatic. The maximum efficiency of LIB operation occurred in a definite temperature range between 20 and 40 °C [1]. To approach this range of temperature, battery cooling is a vital issue. There are two fundamental cooling methods: active methods such as air-cooling and cooling with liquid, passive methods such as phase change material, PCM and heat pipe. Besides, there are two types of cooling, which named internal and external cooling. Al-hallaj and Selman [2] investigated passive thermal management with the aid of PCM. PCM has lower cost and simpler design in comparison with active cooling, but it has a crucial drawback, which can absorb a heat equal to its latent heat. Their results showed that internal cooling has better effects in comparison with external cooling on thermal management of LIB. Giuliano et al. [3] investigated the effects of air-cooling on the thermal management of lithium titanate batteries with high capability by constructing heat exchanger plates, which made with metal foams. Their experiments show using air-cooling systems could be the best effective way for thermal management for automotive battery packs. Also in 2014, the effects of wind tunnel facility on the thermal management of lithium-ion battery modules were studied by He et al. [4] numerically. The comparison of the simulation results with the experimental data shows suitable agreement. After a while, Jin et al. [5] investigated the presence of oblique microchannel heat sinks instead of straight ones. Results showed that oblique microchannel could preserve the surface temperature of the battery below 50 °C for a heat load of 1240 W. One of the most attractive issues to consider in 2014 was the utilization of PCM and to scrutinize the effects of the PCM. Goli et al. [6] focused on the use of hybrid phase change materials with graphene fillers to have heat transfer enhancement and obtained results were satisfactory concerning battery reliability and thermal management. Bandhauer and Garimella [7] investigated the passive cooling method (liquid–vapor phase change processes) as an internal cooling. The weak influence of saturation temperature on the thermal performance of the battery was observed. The application of microchannels embedded in electrodes and cooling with electrolyte was studied for the first time by Mohammadian et al. [8]. It was concluded that internal cooling has better effects on maximum temperature and standard deviation temperature compared to external cooling. Fathabadi [9] studied a cooling system which consists of both active and passive methods concurrently. Distributed and thin air duct and phase change material involved in active and passive cooling, respectively. It was demonstrated that this method has considerable effects on battery charge and discharge performance and battery life cycle. Overall, internal cooling can have a better effect on battery performance and thermal management. Moreover, the uniformity of temperature can affect not only the performance but also the battery efficiency. Another cooling method, which researchers have always explored that, is the utilization of porous media and a combination of porous media with other ways of cooling. In general, for the usage of porous media, some researches have been carried out in recent years. For instance, Siavashi and Maghsoudi [10] studied application of heterogeneous porous media in the lid-driven cavity. They discovered that using this kind of porous media in combination with nanofluids could improve heat transfer up to 8.3%. Zhao [11] simulated fluid flow in a two-dimensional sudden expansion with respect to porous media inserts. It was observed that porous cover permeability tuning results in good heat transfer achievement. In another work, the role of porous media on mixed convection for partially porous square enclosure was investigated by Siavashi et al. [12]. They concluded that Darcy number is a crucial parameter which leads to better heat transfer. The porous heat sink has been always favorable. Since Siavashi and Rasam [13] investigated nanofluid impingement cooling of a cylindrical porous heat sink, their results indicate that increase in the porosity of the porous media will reduce the

temperature profile due to decrease in the shear stress on the wall. Multilayered porous foams have been used by Asiaei and Siavashi [14] to investigate its effects on entropy generation and heat transfer of mixed convection of nanofluid inside a two-sided lid-driven cavity flow heating internally. Their results show that increment of volume fraction results in the decrement of entropy generation. Izadi and Siavashi [15] studied the effects of air, hydrogen and Cu–water nanofluid as cooling fluids while impinged uniformly and non-uniformly on the heat sink covered with porous media. Their results demonstrate that the utilization of non-uniform impinging jet enhances the thermal performance. Utilizing of wedge-shaped porous in front of cylinders and external nanofluid flow over a cylinder has been investigated by Siavashi et al. [16]. The enhancement of heat transfer with an increasing permeable region is observed in their study. Mousavi et al. [17] have evaluated the compilation of nano-PCM, radial fins, to investigate the performance of melting in thermal energy storage. They observed that melting time can be improved by about 28.3% when nano-PCM and radial fins utilize concurrently. Other researchers also have explored in porous media and compilation with other methods. Superposition of porous medium with CuO–water nanofluid in a partitioned square cavity was studied by Selimefendigil et al. [18]. With the aid of the angular rotation speed of the cylinder, significant heat transfer enhancement about 433% was obtained compared to a motionless cylinder. Selimefendigil also explored the effects of cylindrical size and heat transfer enhancement at different Rayleigh numbers for partially layered porous cavity and vertically layered fluid-porous medium enclosure, respectively [19, 20]. Besides, Selimefendigil et al. [21] have studied performance predictions of solar photovoltaic modules equipped with porous fins experimentally. They concluded that utilizing porous fins results in the increment of performance. Sheikholeslami et al. [22] have evaluated electrohydrodynamic nanofluid flow through a porous medium within a wavy chamber to study their effects on thermal transmission. It demonstrates that increment of permeability results in greater thermal transmission and convective circulation. Sheikholeslami et al. [23] investigated the simulation of nanoliquid thermogravitational convective within a porous chamber. They proved that by increasing magnetic forces, convection becomes weaker. Another attractive application of porous media is to cool CPU. Siavashi et al. [24] have studied analytically the effects of magnetic field on the cooling of the porous metal CPU cooler. They conclude that at a low porosity, with increase in the Hartman number slightly, decrease in Nusselt number will be observed. To illustrate the usage of a porous medium in battery application, Mohammadian et al. [25] investigated using of aluminum porous metal foam inside the air-cooled flow channels and thermal management improvement was detected. Also, enhancement of temperature uniformity by utilizing PCM was investigated by Wang et al. [26]. Their results represent that the lower temperature of the Li-ion batteries was guaranteed. Mohammadian and Zhang [27] investigated the influence of metal and non-metal foams on Li-ion battery which has an air-cooled system. They concluded that using partial aluminum foam, which inserted in an airflow channel and partial part of ceramic foam as a heat sink, could keep temperature uniformity in Li-ion battery. There are some researches about utilizing liquid metals. For instance, Yang et al. [28] investigated using liquid metals for Li-ion battery packs. They found that under the same circumstances, liquid metals have a better effect on reduce temperature and increase temperature uniformity compared with water. There are other ways to improve battery thermal management such as battery arrangements and shape optimization. To illustrate the usage of these cooling ways, Park [29] investigated utilizing pressure relief ventilation and tapered manifold to improve thermal management. Also, Xu and He [30] concluded that making the airflow path short by changing the arrangement of the battery from a longitudinal situation to a horizontal situation has acceptable effects on heat dissipation. In 2014, an investigation of installing a fan on top of the battery module effects on cooling performance was studied by Wang et al. [31]. Their results demonstrate that the best cooling performance can be achievable by that installation. They also showed that the cubic arrangement was the best shape according to the cooling expense. Heyhat et al. [32] studied the composition of PCM, nanoparticles, porous metal foams, and fins and their effects on battery thermal management. They conclude that the composition of porous-PCM has the most effect on battery thermal management. Using the porous-PCM can reduce the battery mean temperature by 4–6 K. Optimization has always been favorable among scientists to find the optimal case for their own studies. The purpose of optimization is to achieve the best design relative to a set of prioritized criteria or constraints. Multi-objective optimization used in engineering applications due to the manipulation of more than one objective function to be optimized. One of the algorithms related to multi-objective optimization is non-dominated sorting genetic algorithm. Recently, Abdi and et al. [33] used this algorithm on PEM fuel cell to optimize the operating parameters and find the optimal Pareto front.

In this study, internal cooling plays a role as the determined way of cooling and porous media is considered as an assisted cooling technique. The utilization of porous media in two various configurations was investigated. Inclined porous zone and non-inclined are the two aforementioned configurations. To the best knowledge of the authors, improving thermal management with the aid of porous media in internally cooled Li-ion batteries has been never considered. Also, the parametric study is accomplished

through the response surface method to investigate more data for curve fitting and discover optimum points. The results verify that, with a decrease in porosity, maximum temperature and standard deviation temperature will be reduced. However, the increase in pore size results in maximum temperature and standard deviation decreases.

Problem description

Figure 1 represents a schematic of a unit cell of 5Ah Li-ion battery, which will be analyzed. Due to physical symmetry, to calculate the maximum temperature and standard deviation temperature, only one symmetrical part is considered. As depicted in Fig. 1, there are two microchannels, which determined coolant passing through them. In these microchannels, porous media was inserted. Two different methods of using porous media, which will be analyzed, are sketched in Fig. 1. In the first case, porous zone started to increase from the middle of the inlet cross section to the middle of the outlet cross section. However, in the second case porous zone, it increases from the first point of inlet cross section to the middle of the outlet cross section. Besides, both cases were started from the beginning of cross section and the whole of the microchannel length was filled. This arrangement aims to find out which cases are capable to keep temperature uniformity and also maximum temperature deviation in a proper range to find the optimum case.

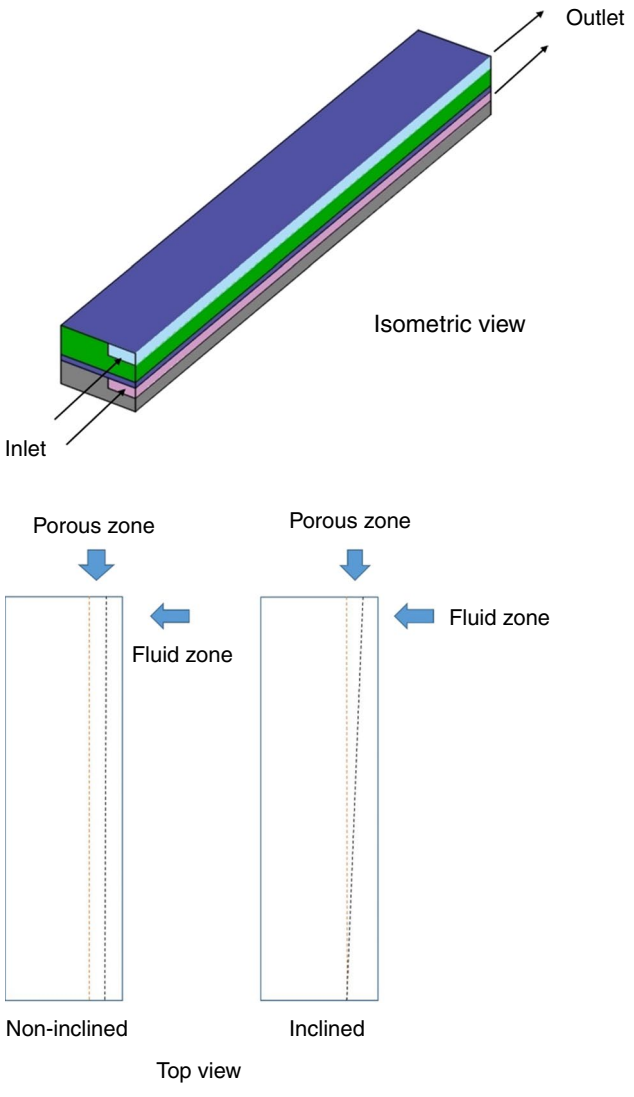

Fig. 1 Problem schematic

Properties of porous media and thermo-physical parameters are tabulated in Table 1. Moreover, boundary conditions are depicted in Fig. 2.

As can be seen in Fig. 2, pressure inlet, pressure outlet and both symmetry are applied as boundary conditions. Dirichlet boundary condition was applied for pressure inlet and pressure outlet. Likewise, the Neumann boundary condition was applied for symmetry. Mathematical forms of applied boundary conditions are as below:

Pressure inlet

$$p_{\text{in}} = p_{\text{static}} + \frac{1}{2}\rho v^2. \tag{1}$$

Pressure outlet

$$p_{\text{out}} = p_{\infty}. \tag{2}$$

Symmetry

$$\frac{\partial \phi}{\partial n} = 0 \tag{3}$$

where ϕ represents all variables at symmetry plane.

The power of coolant pumping through microchannel is calculated as,

$$P = \dot{V}\left(p_{\text{in}} - p_{\text{out}}\right) \tag{4}$$

where $\dot{V}$ is the volumetric flow rate and p_{out} and p_{in} are outlet and inlet pressure of microchannels, respectively.

$$\dot{V} = u_{\text{in}} \cdot A_{\text{in}} \tag{5}$$

where u_{in} and A_{in} are inlet velocity and area of inlet cross section, respectively.

Table 1 Thermo-physical properties of porous media [8]

Material	λ/W m^{-1} K^{-1}	μ/kg m^{-1} s^{-1}
Aluminum	237	–
Brass	109	–
Carbon steel	45	–
Electrolyte ($LiPF_6$)	0.59	0.003

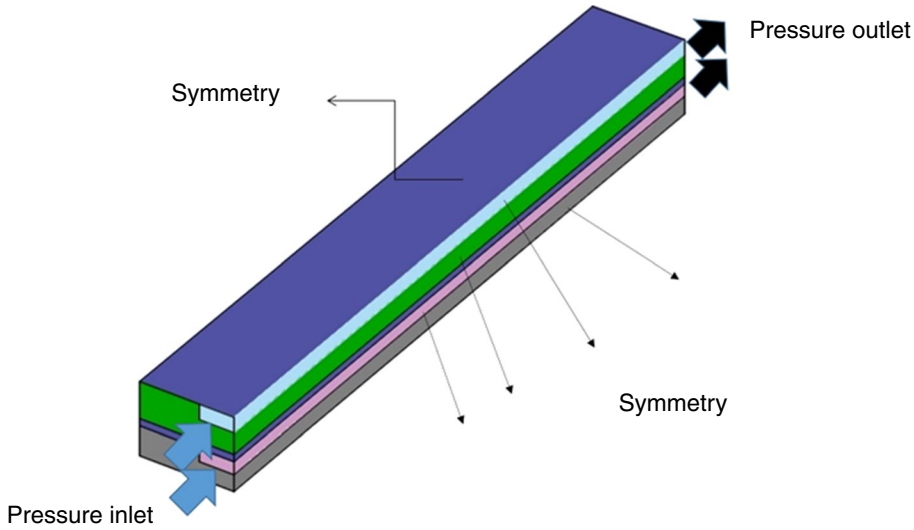

Fig. 2 Boundary conditions

Pumping power is assumed 0.004 W to compare two cases of the porous zone with the non-porous case in terms of temperature uniformity and maximum temperature. Various parts of the typical LIB are lithium metal oxide as the positive terminal and graphite anode as a negative terminal of the battery. Moreover, the electrolyte of the battery contains a compilation of specific organic solvent and lithium salt. Transferring of positive lithium ions occurs during the discharge process; it transports from the negative electrode to the positive electrode through the electrolyte, while passing the electrons over the external circuit is occurred in the same direction.

Although LIBs are capable to work in a various range of temperature operations [34], some thermal concerns are always a priority of researchers to sort them out such as thermal runaway and heat generation within a battery operation [35, 36]. Concentration losing owing to species transport, kinetics of interfacial and charged particle driven by Joule heating results in heat generation in LIB [20]. A lot of expressions have been developed to estimate heat generation, but the most common one is the expression which is introduced according to [37]. Applying the thermodynamic energy balance on a whole cell, the aforementioned expression can be derived. This expression includes several factors such as resistive dissipation which causes heat generation, concentration gradients relaxation in the cell, reversible entropic heat and inner chemical reaction [38]. The heat generation expression is defined as below [39]:

$$\dot{Q} = I(U - V) - I\left(T\frac{\mathrm{d}U}{\mathrm{d}T}\right) \tag{6}$$

where $\dot{Q}$ is the heat generation, I is the electric current which passes within the unit cell, V is the cell voltage, U is the voltage of the open-circuit unit cell, and T is the temperature of the cell. In Eq. (6), the first right-hand side term represents the irreversible over potential heat due to Ohmic losses in the cell, mass transfer limitations and charge-transfer overpotentials at the interface. The second term is reversible entropic heat from electrochemical reactions. Thermal radiation, mixing effects and phase change are neglected in this expression [40]. Besides, the occurrence of a sole electrochemical reaction in Li-ion battery was assumed. It is possible to rewrite Eq. (6) in a different shape [9]:

$$\dot{q} = R_{\mathrm{i}} \cdot i^2 - i \cdot T\frac{\Delta S}{F} \tag{7}$$

where $\dot{q}$, R_{i}, i, F and ΔS are the heat generation occurred internally per unit volume rate, the internal equivalent resistance of the unit cell, Li-ion unit cell current of discharge per unit volume, Faraday number (96,485 C mol^{-1}) and entropy change, respectively.

In many cases, $\dot{q}$ is assumed constant parameter and problems are solved. Nonetheless, according to [8], this correlation can show better results due to time dependency.

State of charge, SOC, and temperature can directly affect the internal equivalent resistance of a unit cell; the following expression represents this notion [9]:

$$R_{\mathrm{i}} = \begin{cases} 2.258 \times 10^{-6}\ \mathrm{SOC}^{-0.3952} & T = 20\,^{\circ}\mathrm{C} \\ 1.857 \times 10^{-6}\ \mathrm{SOC}^{-0.2787} & T = 30\,^{\circ}\mathrm{C} \\ 1.659 \times 10^{-6}\ \mathrm{SOC}^{-0.1692} & T = 40\,^{\circ}\mathrm{C} \end{cases} \tag{8}$$

Hence, the entropy change is calculated as [8]:

$$\Delta S = \begin{cases} 99.88\mathrm{SOC} - 76.67 & 0 \le \mathrm{SOC} \le 0.77 \\ 30 & 0.77 \le \mathrm{SOC} \le 0.87 \\ -20 & 0.77 \le \mathrm{SOC} \le 0.87 \end{cases} \tag{9}$$

where SOC is defined as:

$$\mathrm{SOC} = 1 - \frac{I \cdot t}{C_0} \tag{10}$$

where C_0 (=5 Ah) is the electric capability of the battery and t is the discharge time.

Separator and electrodes are assumed solid. Furthermore, it is assumed that microchannels, which electrolyte flows through to cool battery, were embedded inside the battery cells, the porous zone was inserted in microchannels, and fluid flows inside microchannels do not affect the battery electrochemical performance.

Governing equations

Continuity, momentum and energy equations used to solve the heat transfer problem inside of the battery. The following assumptions are involved in the solution: (1) transient and incompressible flow of electrolyte, (2) homogeneous properties of the porous medium in all directions.

The energy equation and continuity equations for both porous and non-porous cell zones are as follows.

Energy equation

$$\frac{\partial}{\partial t}\left(\gamma\rho_{\mathrm{f}}E_{\mathrm{f}} + (1-\gamma)\rho_{\mathrm{s}}E_{\mathrm{s}}\right) + \nabla\cdot\left(\vec{v}\left(\rho_{\mathrm{f}}E_{\mathrm{f}} + p\right)\right) = \nabla\cdot\left[k_{\mathrm{eff}}\nabla T - \left(\sum hJ\right) + \left(\overline{\overline{\tau}}\cdot\vec{v}\right)\right] + S_{\mathrm{f}}^{h} \tag{11}$$

where k_{eff} is the effective thermal conductivity of the medium $\vec{v}$ is the velocity vector, E_{s} is the total solid medium energy, γ is the porosity of the medium, E_{f} is the total fluid energy, $\overline{\overline{\tau}}$ is the stress tensor, h, is the sensible enthalpy, $S_{\mathrm{f}}^{\mathrm{h}}$ is the source term, J is the diffusion flux, and k_{eff} is calculated as below:

$$k_{\mathrm{eff}} = \gamma k_{\mathrm{f}} + (1-\gamma)k_{\mathrm{s}} \tag{12}$$

where k_{s} is the thermal conductivity of the solid medium, and k_{f} is the thermal conductivity of the fluid phase, Other governing equations presented as follows:

$$\frac{\partial\rho_{\mathrm{f}}}{\partial t} + \nabla\cdot\left(\rho_{\mathrm{f}}\vec{v}\right) = 0 \tag{13}$$

$$\frac{\partial}{\partial t}\left(\rho_{\mathrm{f}}\vec{v}\right) + \nabla\cdot\left(\rho_{\mathrm{f}}\vec{v}\vec{v}\right) = -\nabla p + \nabla\cdot\left(\overline{\overline{\tau}}\right) + \rho\vec{g} + \vec{S} \tag{14}$$

where $\vec{S}$ is the source term and p is the static pressure. Source term is defined as:

$$\vec{S} = -\left(\sum D\mu\vec{v} + \sum C\frac{1}{2}\rho|v|\vec{v}\right) \tag{15}$$

where $C, |v|$ and D are inertial resistance, velocity magnitude and viscous resistance, respectively. Inertial and viscous resistance is defined as below [41]:

$$D = \frac{\gamma^2}{K} \tag{16}$$

$$C = \frac{2C_{\mathrm{F}}\gamma^3}{\sqrt{K}} \tag{17}$$

where C_{F} is the inertial coefficient and K is the permeability. The main non-dimensional parameters defined as follows.

Nusselt number

$$\mathrm{Nu} = \frac{h_{\mathrm{c}}D_{\mathrm{h}}}{k_{\mathrm{eff}}} \tag{18}$$

where h_{c} is convective coefficient and D_{h} is the hydraulic diameter.

Reynolds number

$$\mathrm{Re} = \frac{v_{\mathrm{f}}D_{\mathrm{h}}}{\nu_{\mathrm{f}}} \tag{19}$$

where v_{f} is the fluid velocity, and ν_{f} is kinematic viscosity.

Prandtl number

$$\mathrm{Pr} = \frac{\nu_{\mathrm{f}}}{\alpha} \tag{20}$$

where α is thermal diffusivity.

Darcy number

$$\mathrm{Da} = \frac{K}{D_{\mathrm{h}}^2} \tag{21}$$

Numerical solution and model validation

Second-order transient and pressure-based solver was used to simulate both cases of the porous zones. The PISO scheme was utilized for the pressure–velocity coupling, due to the rate of convergency compared to the SIMPLE approach for transient flows. Utilizing a PISO scheme results in number of iteration decrement to approach convergence [42]. Governing equations were discretized with the second-order upwind scheme. To make sure about convergency, scaled residuals monitoring is crucial. Residuals were set to be below 10^{-14}; also the time step size was set to be one second. UDF code was written due to the time dependency of battery heat generation.

Four different grids were evaluated to study grid sensitivity. The maximum temperature in each grid was compared due to grid sensitivity analysis to find the proper grid. The

Table 2 Grid independency at pumping power = 4×10^{-2} W, discharge rate = 5C and SOC = 0.167

Number of elements	Maximum temperature/K	Relative error %	Velocity/m s^{-1}	Relative error %
810,000	308.13		0.9407	
1,360,000	308.24	0.035	0.94089	0.017
1,780,000	308.48	0.077	0.9415	0.054
2,114,000	308.44	−0.01	0.94145	−0.0045

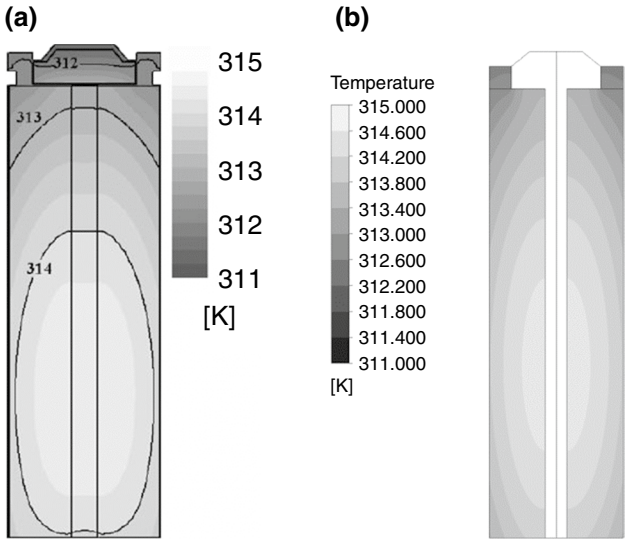

Fig. 3 Comparison of the temperature distribution in **a** temperature distribution of model in [43]. **b** Temperature distribution of numerical investigation with using of proposed UDF

grid independency was accomplished under the following conditions: 15 kPa inlet pressure and 27 °C inlet temperature to achieve desirable pumping power of 4×10^{-2} W. The results were calculated for those circumstances which were above mentioned and other conditions like SOC = 0.167 and 5C discharge rate. The simulation results are tabulated in Table 2. It is observed that the 1,780,000 cells would be appropriate.

As the heat generation inside the battery varies with time, heat generation should be computed in time. To validate the proposed UDF, it was studied numerically in the simulation of temperature distribution in a small size of SONY-US18650GS [43]. Figure 3a depicts the temperature distribution in cylindrical battery [43], and Fig. 3b shows the result of proposed UDF. There is a good agreement between the temperature distribution in [43] and the proposed numerical simulation. Results show that the difference between their maximum temperatures is no more than 0.2%.

Hence, to validate the numerical solution method, numerical results of [8] were used and all data are summarized in Table 3. It represents that there is an excellent agreement between the results of the present study and the data reported in [8].

Table 3 Model validation at pumping power = 4×10^{-2} W and discharge rate = 5C

SOC	Temperature/K (present study)	Temperature/K ([8])	Error %
1	300	300	0.37
0.7	306.19	305.067	0.37
0.6	306.26	305.136	0.37
0.2	308.48	307.336	0.37

Table 4 Time step size independency at pumping power = 4×10^{-2} W, discharge rate = 5C and SOC = 0.167

Time step size/s	Maximum temperature/K	Relative error %
0.5	308.47	0.0032
1	308.48	0.0016
1.5	308.485	

Moreover, time step size independency test has been carried out and three different time steps were explored to evaluate the sensitivity of maximum temperature. This evaluation is tabulated entirely in Table 4.

Results and discussion

This study aimed to determine the effective configuration of the porous zone and discover optimum parameters, which could be led the better LIB pack performance in terms of improving standard deviation temperature and the bulk temperature reduction inside the battery pack, i.e., in the hybrid electric vehicles. STD is calculated as below

$$\mathrm{STD} = \sqrt{\frac{\sum_{j=1}^{N} \left(T_{\mathrm{j}} - T_{\mathrm{ave}}\right)^2}{N-1}} \tag{22}$$

where N, T_{j} and T_{ave} are the number of computational cells, the temperature of each of computational cell and average temperature, respectively.

STD is used to describe the temperature uniformity. Temperature uniformity is about one of the crucial factors to consider devising a proper LIB pack, which can work in the optimum range. Aging is one of the key factors that makes the temperature non-uniformity. Aging results in a thermal imbalance in cells, and it decreases battery performance.

Increment of surface contact in heat exchanging is one of the efficient works for heat transfer augmentation. So that utilizing porous media has always been considerable. In the present study, in the first case porous zone was utilized in mid of microchannels, and in the second case, the porous zone was utilized obliquely. After simulation in the non-inclined porous zone, it can find a cooling efficiency for maximum temperature and standard deviation temperature. Cooling efficiency is calculated as below:

$$\mathrm{CE}\,(\%) = \frac{T_{\mathrm{max,P}} - T_{\mathrm{max,np}}}{T_{\mathrm{max,np}} - 300} \times 100 \tag{23}$$

where $T_{\mathrm{max,P}}$ and $T_{\mathrm{max,np}}$ are the maximum temperature of battery in the presence of porous media and maximum temperature of battery in the absence of porous media, respectively. It can be written for STD like the aforementioned cooling efficiency formulation.

$$\mathrm{CE}\,(\%) = \frac{\mathrm{STD_p} - \mathrm{STD_{np}}}{\mathrm{STD_{np}} - 0} \times 100 \tag{24}$$

where $\mathrm{STD_{,p}}$ and $\mathrm{STD_{,np}}$ are temperature standard deviation of the battery in the presence of porous media and temperature standard deviation of the battery in the absence of porous media, respectively.

According to Eqs. (23) and (24), the presence of porous media can enhance maximum temperature and STD, 8.72% and 7.5%, respectively.

Lesser STD can result in better battery performance and increment of the battery life cycle. Besides, in inclined porous zone configuration, the temperature difference in the inlet of microchannels, which heat-transferring contact surface is higher than the outlet, is lower and this temperature difference in the outlet of microchannels is higher than inlets. It seems desirable and because of that, a new simulation was explored to study the effects of inclined porous zone configuration on maximum temperature and STD compared to the non-inclined porous zone. This comparison is given in Figs. 4 and 5.

Figures 4 and 5 show the maximum temperature and standard deviation temperature versus state of charge at constant pumping power = 0.004 W and 5C discharge rate, respectively to find optimum case between inclined and non-inclined porous zone configuration. Their results depict that utilizing an inclined porous zone configuration can improve both maximum temperature and temperature uniformity. Figure 5 shows that temperature uniformity, which is a key factor to improve battery efficiency, decreases significantly by about 27.02%. It means that an inclined porous zone can consider optimum configuration to battery cooling and owing to reduce the computational cost, other influential parameters can be studied only in this case. In addition, it can be found that the variation of the state of charge causes the variation of temperature as can be seen as the peak of the curve is in SOC = 0.2. It means when the battery is about fully discharged, the temperature reaches its maximum state.

Velocity contour in the vicinity of the unit cell battery outlet region in the inclined porous configuration is shown in Fig. 6. The maximum velocity and maximum velocity gradient are in the vicinity of the outlet region.

To choose the optimum geometry of porous media for battery cooling, three other important parameters were considered. It is required to use some methodologies to discover how these three parameters can affect the battery cooling

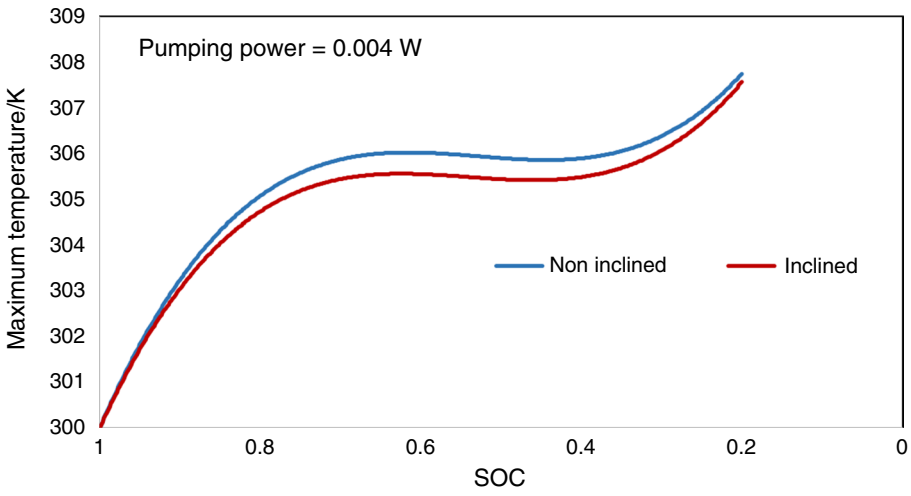

Fig. 4 Maximum temperature inside the battery versus state of charge

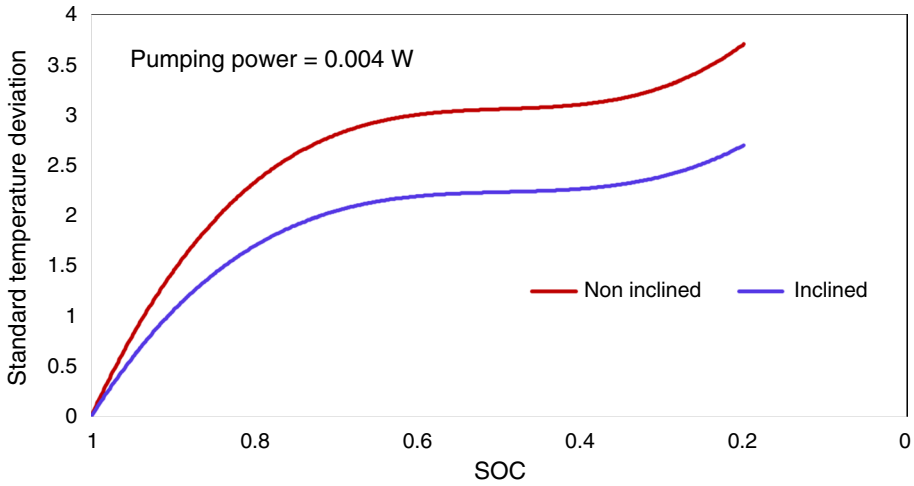

Fig. 5 Standard deviation temperature field versus state of charge

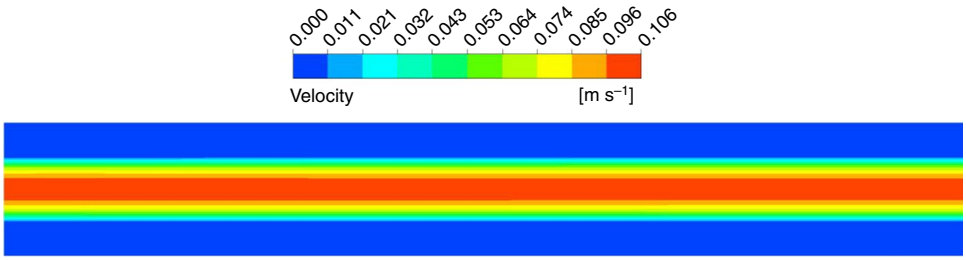

Fig. 6 Velocity variation at the outlet region of lithium-ion battery unit cell

and find the optimal point. With consideration of nonlinearity functions, the response surface method was chosen. The response surface method is a statistical method that is immensely utilized in branches of modeling and processes assessment [44]. This method is based on determining surface placement. Thus, the main purpose of the response surface method is to discover the topology of the response surface including local and relative extremums, and find the most suitable location for an optimal answer [45]. This method is applied to investigate a good approximate correlation for inputs and outputs. Also, the designation of optimum operating conditions with the satisfaction of constraints is possible through this method [46, 47]. Experimental data is evaluated to be fitted in a proper model. Model coefficients are presented with constant parameters, interactive coefficients and quadratic coefficients. Adequate precision, adjusted determination coefficient (Adj-R^2) and correlation coefficient (R^2) are utilized to verify the adequacies of the model; when the following conditions are satisfied, the model can be adequate: lack of fit P value > 0.05, adequate precision > 4, P value < 0.05 and $R^2 > 0.9$. To analysis of variance, testing of differences between means can be carried out [48]. One of the most crucial applications of response surface method is in design of experiments. Advantage of the design of experiments utilizing is reducing of required tests. Nevertheless, the lack of accuracy in some limited cases is observed [49, 50].

The central composite design is used to prepare the design table. Some results of the simulation are given in Figs. 7–9. Figure 7 shows the effect of different materials for the solid part of the porous zone on the maximum temperature inside the battery pack. It demonstrates that aluminum due to its thermal conductivity could be led the battery pack to perform in a fewer temperature variation.

Figure 8 also shows the maximum temperature versus the state of charge inside the battery, and the aim of sketching this plot was discovering the role of pore size variation in improving maximum temperature and temperature uniformity. Material and porosity were considered constant. As can be seen, with an increase in pore size, the maximum temperature will be reduced. It seems that the maximum temperature can be improved by about 20.75%.

Figure 9 depicts the maximum temperature versus the state of charge inside the battery. Material and pore size were considered constant. Figure 9 shows with a decrease in porosity, the maximum temperature will be reduced and compared to Figs. 8 and 9; it can be found that porosity has a better effect on maximum temperature compared to pore size. The maximum temperature can be improved concerning porosity about 24.88%.

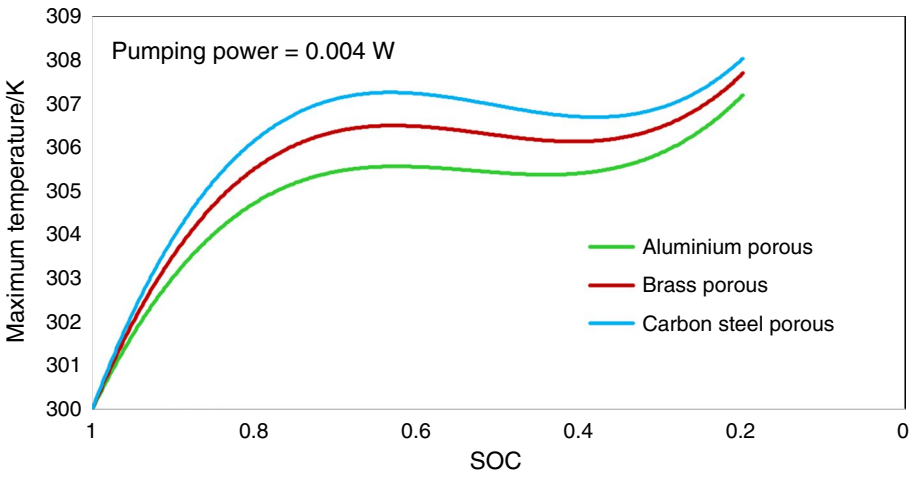

Fig. 7 Maximum temperature versus state of charge for different materials, porosity = 0.5 and pore size = 10 μm for the solid part of the inclined porous zone

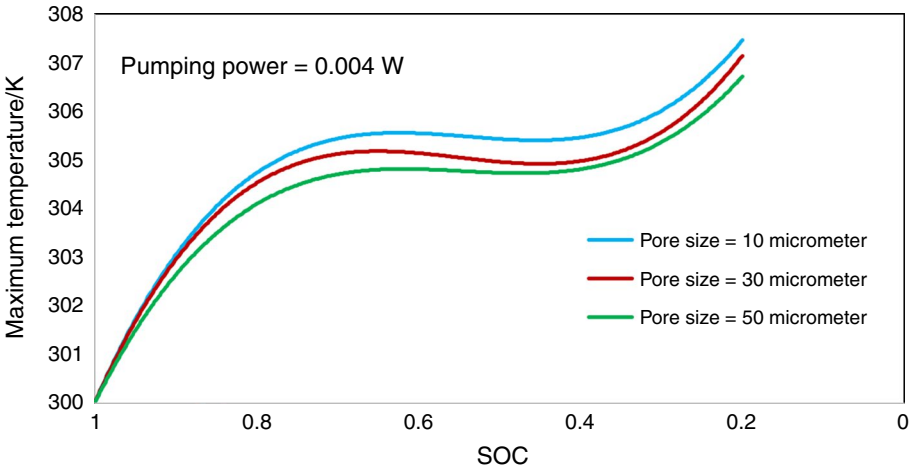

Fig. 8 Maximum temperature versus state of charge for different pores size, aluminum porous material and porosity = 0.65 of the inclined porous zone

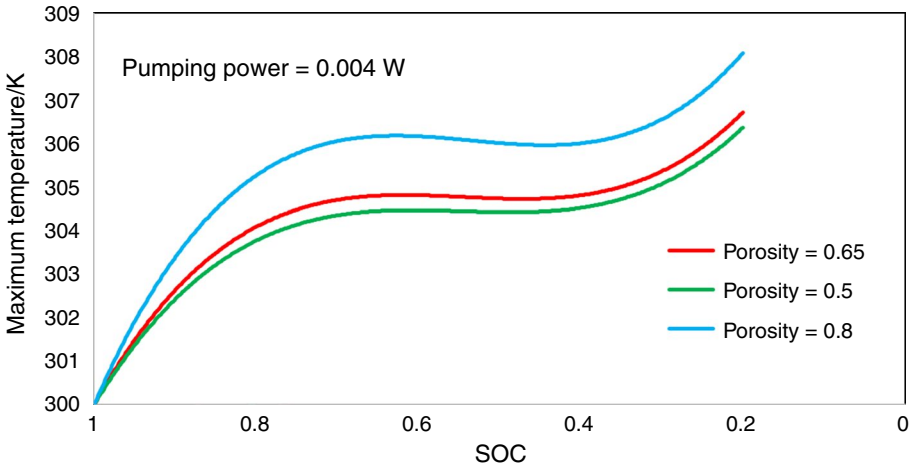

Fig. 9 Maximum temperature versus state of charge for different porosities, aluminum porous material and pore size = 10 μm of the inclined porous zone

STD and maximum temperature were considered as objective functions, and statistical investigation results were categorized into two groups. Results of maximum temperature investigation as a response variable are given in Figs. 10, 11 and Tables 4, 5. Also, the results of the STD investigation as a response variable are given in Figs. 11, 12 and Tables 6, 7.

Tables 5 and 7 show the success percentage of fitted data and prediction modeling for maximum temperature and standard temperature deviation, respectively. It is

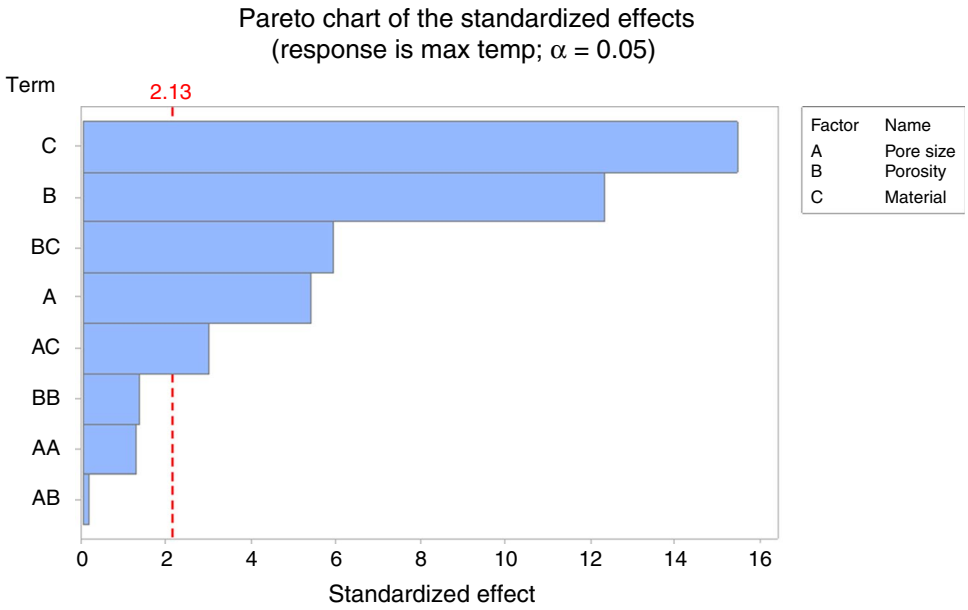

Fig. 10 Effects of different factors on maximum temperature

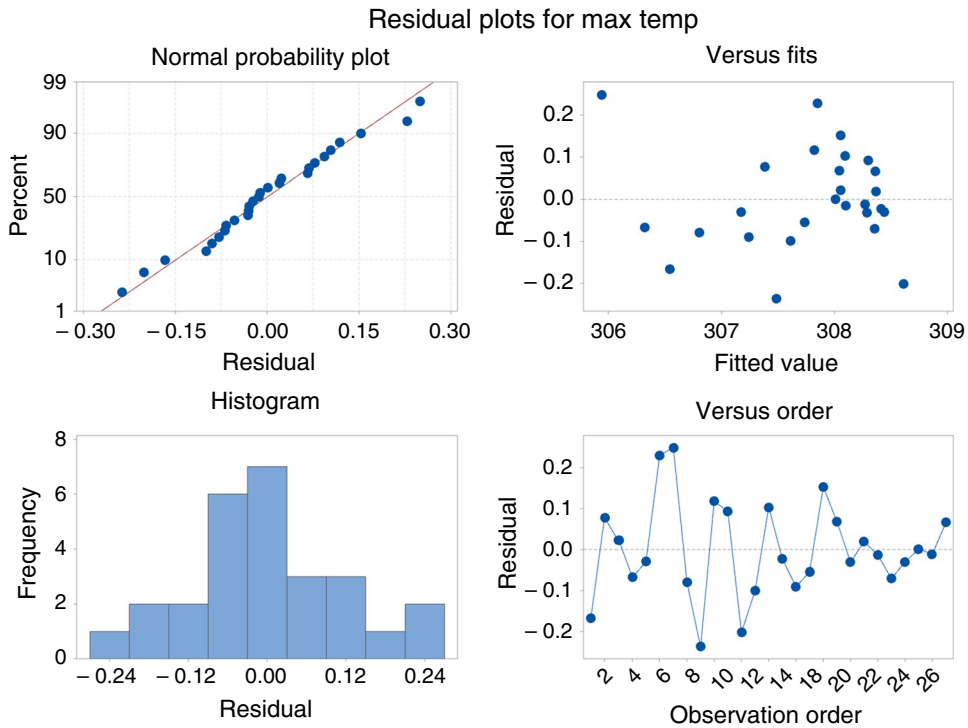

Fig. 11 Statistical plots of maximum temperature optimization modeling

Table 5 The success percentage of fitted data and prediction model for maximum temperature

R^2	R^2 (predict)
97.32%	88.22%

obvious from the table that both prediction and fitted data were carried out successfully and the following results will be trustable.

Figures 9 and 11 show the Pareto plots, which study parameters versus standardized effects for maximum temperature and standard temperature deviation, respectively. It demonstrates that the most effective parameter on maximum temperature is porous media material. In the next places, porosity, the interaction of porosity and material, pore size, interaction of pore size and material are important parameters, respectively. The point is the interaction of porosity and material is more important than the main effect of pore size.

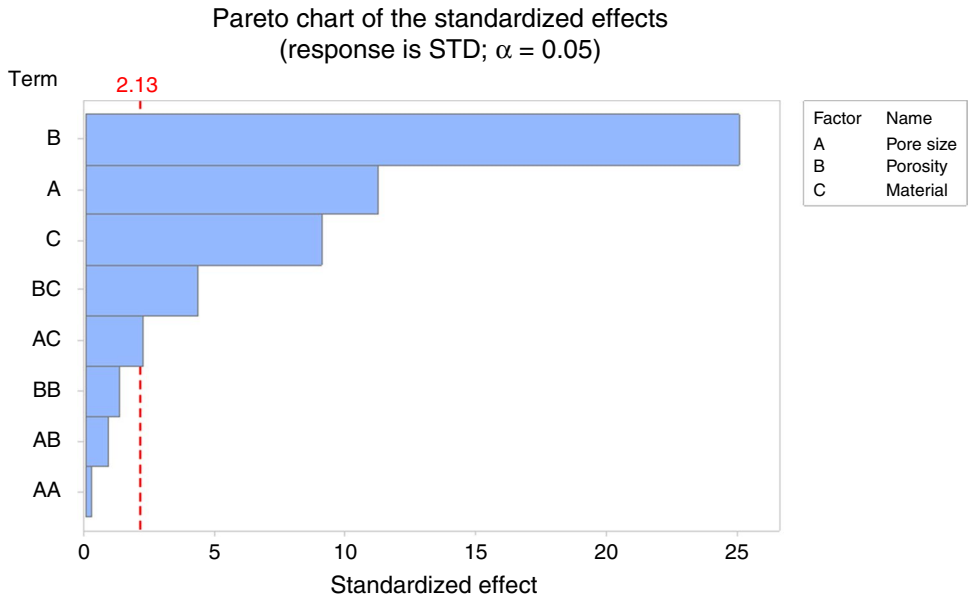

Fig. 12 Effects of different factors on standard deviation temperature

Table 6 Optimum maximum temperature correlation for different materials

Material	Correlation
Aluminum	$\text{Max Temp} = 302.55 - 0.0042 \times \text{PS} + 9.97 \times \text{PO} - 0.000197 \times \text{PS} \times \text{PS} - 3.79 \times \text{PO} \times \text{PO} + 0.0022 \times \text{PS} \times \text{PO}$
Brass	$\text{Max Temp} = 305.05 - 0.0039 \times \text{PS} + 7.54 \times \text{PO} - 0.000197 \times \text{PS} \times \text{PS} - 3.79 \times \text{PO} \times \text{PO} + 0.0022 \times \text{PS} \times \text{PO}$
Carbon steel	$\text{Max Temp} = 305.90 + 0.0098 \times \text{PS} + 6.00 \times \text{PO} - 0.000197 \times \text{PS} \times \text{PS} - 3.79 \times \text{PO} \times \text{PO} + 0.0022 \times \text{PS} \times \text{PO}$

Table 7 The success percentage of the fitted data and prediction model for STD

R^2	R^2 (predicted)
98.36%	93.10%

In addition, it can demonstrate that for STD, which, porosity is the most effective parameter on STD, pore size, material, and the interaction of porosity and material, interaction of pore size and material are the other effective parameters.

Figures 11 and 13 show the statistical plots for maximum temperature and standard deviation temperature, respectively. These two figures illustrate residual and error, which resulted from data fitting. The error between real data and fitted line, based on the response surface method, is so negligible, and residuals are so close to Gaussian distribution, which can be concluded that errors from simulation were random.

Correlations of the fitted diagram on simulation data concerning different materials are given in Tables 6 and 8 for maximum temperature and STD, respectively, through these correlations and just between the given range of porosity, pore size and material. To approach the more concise correlations, it can be possible to eliminate ineffective parameters and reinvestigate. Nevertheless, it was neglected owing to the importance of accuracy

Figure 14 also depicts the main effects of the proposed parameters and how they can influence the maximum temperature and standard temperature deviation. It demonstrates that changing material has the most influence on maximum temperature. However, porosity seems that it is a crucial factor in improving the standard temperature deviation.

After the parametric study, analysis of simulation results and discover the model to describe the STD and maximum temperature based on effects of material, porosity and pore size and their interactions, finding the optimum case of these parameters to minimize the STD and maximum temperature to increment of battery performance and battery life cycle was considered. Table 8 shows the optimum case of parameters that were studied. The final solution depicts that composite desirability is one that means both maximum

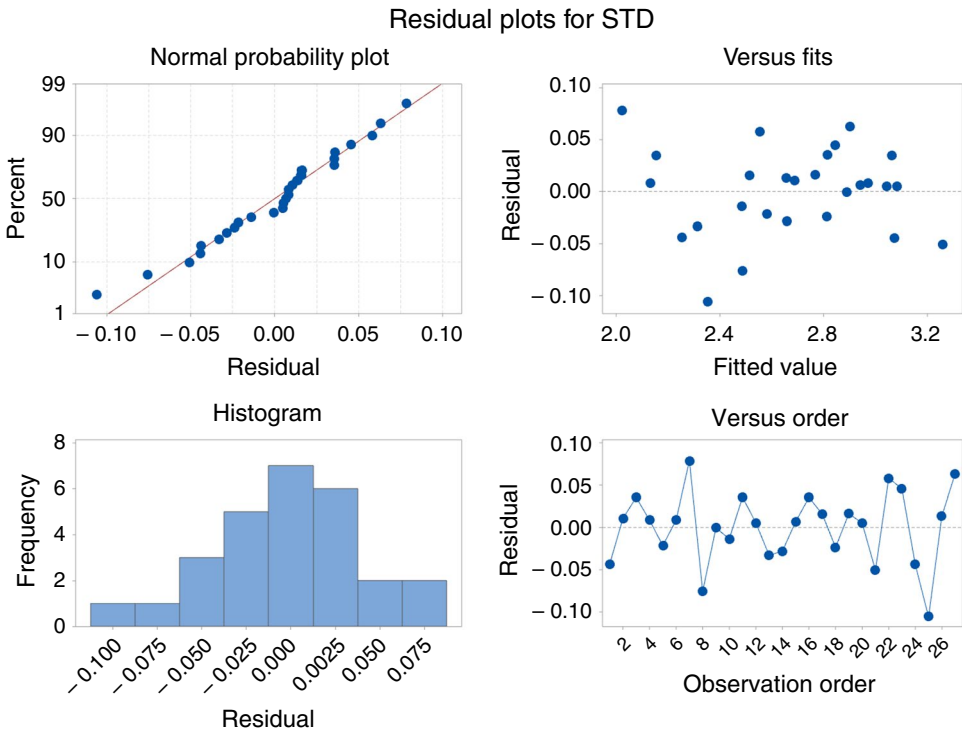

Fig. 13 Statistical plots of standard deviation temperature optimization modeling

Table 8 Optimum STD correlation for different materials

Material	Correlation
Aluminum	$STD = 0.457 - 0.00915 \times PS + 4.39 \times PO + 0.000015 \times PS \times PS - 1.34 \times PO \times PO + 0.00486 \times PS \times PO$
Brass	$STD = 1.061 - 0.01157 \times PS + 3.69 \times PO + 0.000015 \times PS \times PS - 1.34 \times PO \times PO + 0.00486 \times PS \times PO$
Carbon Steel	$STD = 1.549 - 0.01378 \times PS + 3.33 \times PO + 0.000015 \times PS \times PS - 1.34 \times PO \times PO + 0.00486 \times PS \times PO$

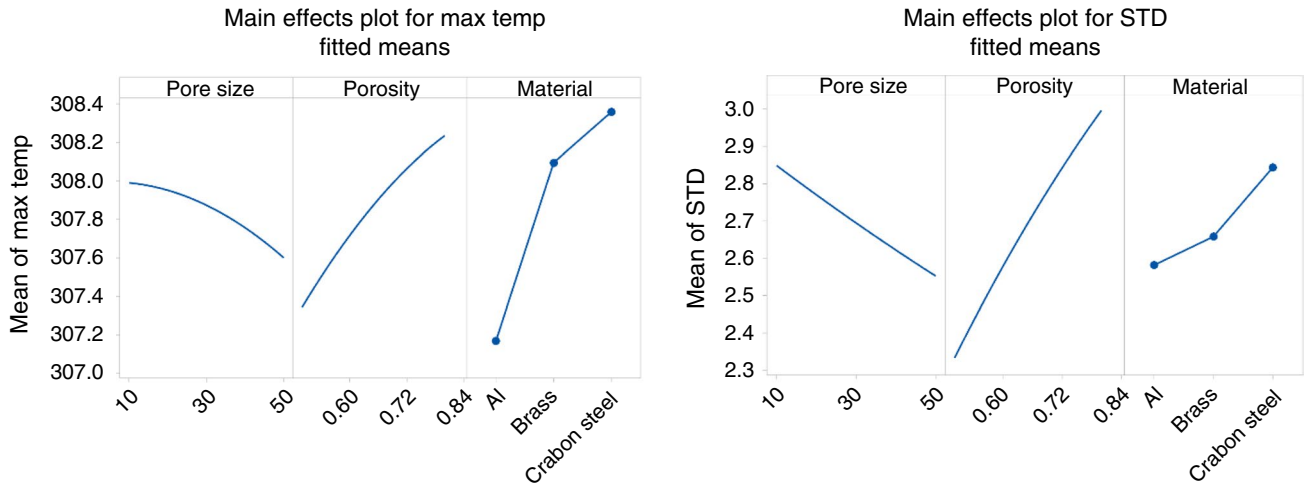

Fig. 14 Main effects for both maximum temperature and standard deviation temperature

Table 9 Final solution

Solution	Pore size	Porosity	Material	STD fit	Max temp fit	Composite desirability
1	50	0.5	Aluminum	2.02129	305.94	1

temperature and STD have aligned behavior and optimized together. It means if every parameter among the studied parameters be able to minimize the maximum temperature that will be able to minimize the STD. With the aid of inclined porous media and properties of Table 9, maximum temperature and STD will be 305.94 °C and 2.02129, respectively, which means cooling efficiency will be 29.95%.

Recommendations and future directions

In general, keeping the maximum temperature and standard deviation temperature as the most crucial parameters in LIB thermal management, in the suitable range, has been always desirable. Numerous techniques have been explored to find an effective way to approach the appropriate thermal efficiency. Some specific recommendations, which can steer the direction of future research, are given below:

1. Thermal energy storage systems such as PCMs have always been favorable to investigate the thermal efficiency of numerous thermal applications. Solidification and melting are the main processes of PCMs. Released/absorbed heat can affect the thermal efficiency. Influences of using PCM on battery thermal management can be investigated.
2. Due to the augment of the heat transfer in thermal applications, using of nanofluids possibly affects the battery thermal system.

Conclusions

The three-dimensional thermal study was performed to explore internally cooled Li-ion battery pack and observation of porous zone effects on battery thermal management. Effects of the utilization of two different configurations of the porous zone, three different materials, three different porosity and three different pore size were investigated. For optimization, the response surface method was utilized. The whole of simulations in constant pumping power and discharge rate resulted in the following results:

- Utilization of porous zone as an assistant to internal cooling, in comparison with the case without the porous insert is that it reduces the maximum temperature inside the battery, what is more, improves the temperature uniformity, which is the most crucial factor for the efficiency of the battery.
- Inclined porous zone makes the Li-ion battery better performance, compared to non-inclined porous zone, especially in terms of temperature uniformity.
- Aluminum is the best material for utilizing in the solid part of the porous zone.
- With a decrease in porosity, maximum temperature and temperature uniformity become improve. However, with an increase in pore size maximum temperature and temperature uniformity become improve.
- Optimum case to approach the best performance in terms of optimum temperature uniformity and optimum maximum temperature is 50-μm pore size, 0.5 porosity and aluminum material for the solid part of the porous zone.

References

1. Kuper C, Hoh M, Houchin-Miller G, Fuhr J. Thermal management of hybrid vehicle battery systems. EVS24, Stavanger, Norway. 2009:1–10.
2. Al Hallaj S, Selman J. A novel thermal management system for electric vehicle batteries using phase-change material. J Electrochem Soc. 2000;147(9):3231–6.
3. Giuliano MR, Prasad AK, Advani SG. Experimental study of an air-cooled thermal management system for high capacity lithium–titanate batteries. J Power Sources. 2012;216:345–52.
4. He F, Li X, Ma L. Combined experimental and numerical study of thermal management of battery module consisting of multiple Li-ion cells. Int J Heat Mass Transf. 2014;72:622–9.
5. Jin L, Lee P, Kong X, Fan Y, Chou S. Ultra-thin minichannel LCP for EV battery thermal management. Appl Energy. 2014;113:1786–94.
6. Goli P, Legedza S, Dhar A, Salgado R, Renteria J, Balandin AA. Graphene-enhanced hybrid phase change materials for thermal management of Li-ion batteries. J Power Sources. 2014;248:37–43.
7. Bandhauer TM, Garimella S. Passive, internal thermal management system for batteries using microscale liquid–vapor phase change. Appl Therm Eng. 2013;61(2):756–69.
8. Mohammadian SK, He Y-L, Zhang Y. Internal cooling of a lithium-ion battery using electrolyte as coolant through microchannels embedded inside the electrodes. J Power Sources. 2015;293:458–66.
9. Fathabadi H. A novel design including cooling media for lithium-ion batteries pack used in hybrid and electric vehicles. J Power Sources. 2014;245:495–500.
10. Maghsoudi P, Siavashi M. Application of nanofluid and optimization of pore size arrangement of heterogeneous porous media to enhance mixed convection inside a two-sided lid-driven cavity. J Therm Anal Calorim. 2019;135(2):947–61.
11. Zhao Z. Numerical modeling and simulation of heat transfer and fluid flow in a two-dimensional sudden expansion model using

porous insert behind that. J Therm Anal Calorim. 2020. https://doi.org/10.1007/s10973-020-09505-1.
12. Siavashi M, Karimi K, Xiong Q, Doranehgard MH. Numerical analysis of mixed convection of two-phase non-Newtonian nanofluid flow inside a partially porous square enclosure with a rotating cylinder. J Therm Anal Calorim. 2019;137(1):267–87.
13. Siavashi M, Rasam H, Izadi A. Similarity solution of air and nanofluid impingement cooling of a cylindrical porous heat sink. J Therm Anal Calorim. 2019;135(2):1399–415.
14. Asiaei S, Zadehkafi A, Siavashi M. Multi-layered porous foam effects on heat transfer and entropy generation of nanofluid mixed convection inside a two-sided lid-driven enclosure with internal heating. Transp Porous Media. 2019;126(1):223–47.
15. Izadi A, Siavashi M, Xiong Q. Impingement jet hydrogen, air and CuH_2O nanofluid cooling of a hot surface covered by porous media with non-uniform input jet velocity. Int J Hydrog Energy. 2019;44(30):15933–48.
16. Siavashi M, Iranmehr S. Using sharp wedge-shaped porous media in front and wake regions of external nanofluid flow over a bundle of cylinders. Int J Numer Methods Heat Fluid Flow. 2019;29:3730–55.
17. Mousavi S, Siavashi M, Heyhat MM. Numerical melting performance analysis of a cylindrical thermal energy storage unit using nano-enhanced PCM and multiple horizontal fins. Numer Heat Transf Part A Appl. 2019;75(8):560–77.
18. Selimefendigil F, Ismael MA, Chamkha AJ. Mixed convection in superposed nanofluid and porous layers in square enclosure with inner rotating cylinder. Int J Mech Sci. 2017;124:95–108.
19. Chamkha AJ, Selimefendigil F, Ismael MA. Mixed convection in a partially layered porous cavity with an inner rotating cylinder. Numer Heat Transf Part A Appl. 2016;69(6):659–75.
20. Ismael MA, Selimefendigil F, Chamkha AJ. Mixed convection in a vertically layered fluid-porous medium enclosure with two inner rotating cylinders. J Porous Media. 2017;20(6):491–511.
21. Selimefendigil F, Bayrak F, Oztop HF. Experimental analysis and dynamic modeling of a photovoltaic module with porous fins. Renew Energy. 2018;125:193–205.
22. Sheikholeslami M, Sheremet MA, Shafee A, Li Z. CVFEM approach for EHD flow of nanofluid through porous medium within a wavy chamber under the impacts of radiation and moving walls. J Therm Anal Calorim. 2019;138(1):573–81.
23. Sheikholeslami M, Sheremet MA, Shafee A, Tlili I. Simulation of nanoliquid thermogravitational convection within a porous chamber imposing magnetic and radiation impacts. Physica A Stat Mech Appl. 2020. https://doi.org/10.1016/j.physa.2019.124058.
24. Izadi A, Siavashi M, Rasam H, Xiong Q. MHD enhanced nanofluid mediated heat transfer in porous metal for CPU cooling. Appl Therm Eng. 2020;168:114843.
25. Mohammadian SK, Rassoulinejad-Mousavi SM, Zhang Y. Thermal management improvement of an air-cooled high-power lithium-ion battery by embedding metal foam. J Power Sources. 2015;296:305–13.
26. Wang Z, Zhang Z, Jia L, Yang L. Paraffin and paraffin/aluminum foam composite phase change material heat storage experimental study based on thermal management of Li-ion battery. Appl Therm Eng. 2015;78:428–36.
27. Mohammadian SK, Zhang Y. Temperature uniformity improvement of an air-cooled high-power lithium-ion battery using metal and non-metal foams. J Heat Transf. 2016;138(11):114502.
28. Yang X-H, Tan S-C, Liu J. Thermal management of Li-ion battery with liquid metal. Energy Convers Manag. 2016;117:577–85.
29. Park H. A design of air flow configuration for cooling lithium ion battery in hybrid electric vehicles. J Power Sources. 2013;239:30–6.
30. Xu X, He R. Research on the heat dissipation performance of battery pack based on forced air cooling. J Power Sources. 2013;240:33–41.
31. Wang T, Tseng K, Zhao J, Wei Z. Thermal investigation of lithium-ion battery module with different cell arrangement structures and forced air-cooling strategies. Appl Energy. 2014;134:229–38.
32. Heyhat MM, Mousavi S, Siavashi M. Battery thermal management with thermal energy storage composites of PCM, metal foam, fin and nanoparticle. J Energy Storage. 2020;28:101235.
33. Abdi H, Messaoudene AN, Kolsi L, Belazzoug M. Multi-objective optimization of operating parameters of a PEM fuel cell under flooding conditions using the non-dominated sorting genetic algorithm (NSGA-II). Therm Sci. 2019;23:3525–37.
34. Nishi Y. Lithium ion secondary batteries; past 10 years and the future. J Power Sources. 2001;100(1–2):101–6.
35. Lisbona D, Snee T. A review of hazards associated with primary lithium and lithium-ion batteries. Process Saf Environ Prot. 2011;89(6):434–42.
36. Feng Z, Zhang Y. Safety monitoring of exothermic reactions using time derivatives of temperature sensors. Appl Therm Eng. 2014;66(1–2):346–54.
37. Bernardi D, Pawlikowski E, Newman J. A general energy balance for battery systems. J Electrochem Soc. 1985;132(1):5–12.
38. Bhatia PC. Thermal analysis of lithium-ion battery packs and thermal management solutions. Columbus: The Ohio State University; 2013.
39. Gu W, Wang C. Thermal-electrochemical modeling of battery systems. J Electrochem Soc. 2000;147(8):2910–22.
40. Bandhauer TM. Electrochemical-thermal modeling and microscale phase change for passive internal thermal management of lithium ion batteries. Atlanta: Georgia Institute of Technology; 2011.
41. Clearman WM. Measurement and correlation of directional permeability and Forchheimer's inertial coefficient of micro porous structures used in pulse tube cryocoolers. Atlanta: Georgia Institute of Technology; 2007.
42. Jones DA, Clarke D. Simulation of flow past a sphere using the fluent code: defense science and technology organization victoria (australia) maritime; 2008.
43. Inui Y, Kobayashi Y, Watanabe Y, Watase Y, Kitamura Y. Simulation of temperature distribution in cylindrical and prismatic lithium ion secondary batteries. Energy Convers Manag. 2007;48(7):2103–9.
44. Braimah MN, Anozie AN, Odejobi OJ. Utilization of response surface methodology (RSM) in the optimization of crude oil refinery process, new Port-Harcourt Refinery, Nigeria. J Eng Sci Technol. 2016;3:4361–9.
45. Bradley N. The response surface methodology. South Bend: Indiana University South Bend; 2007.
46. Farooq Z, Rehman Su, Abid M. Application of response surface methodology to optimize composite flour for the production and enhanced storability of leavened flat bread (Nan). J Food Process Preserv. 2013;37(5):939–45.
47. Pishgar-Komleh S, Keyhani A, Mostofi-Sarkari M, Jafari A. Application of response surface methodology for. Iran J Energy Environ. 2012;3(2):134–42.
48. Aydar A, Bağdatlıoğlu N, Köseoğlu O. Effect of ultrasound on olive oil extraction and optimization of ultrasound-assisted extraction of extra virgin olive oil by response surface methodology (RSM). Grasas Aceites. 2017;68(2):189.
49. Boyacı İH. A new approach for determination of enzyme kinetic constants using response surface methodology. Biochem Eng J. 2005;25(1):55–62.
50. Koç B, Kaymak-Ertekin F. Response surface methodology and food processing applications. GIDA J Food. 2010;35(1):63–70.